Journal of
Nanotheranostics

MDPI

Article

Exploring the Role of Fibroblasts in Promoting Neuroblastoma Cell Migration and Invasion

Diana Corallo [1,*,†], Cristina Nardelli [1,†], Marcella Pantile [1], Sara Menegazzo [1,2], Alessandra Biffi [2] and Sanja Aveic [1]

[1] Laboratory of Target Discovery and Biology of Neuroblastoma, Istituto di Ricerca Pediatrica Fondazione Città della Speranza, 35127 Padova, Italy; cristina.nardelli.1@studenti.unipd.it (C.N.); m.pantile@irpcds.org (M.P.); sara.menegazzo.3@phd.unipd.it (S.M.); s.aveic@irpcds.org (S.A.)
[2] Division of Pediatric Hematology, Oncology, and Stem Cell Transplant, Department of Woman's and Child's Health, Padua University Hospital, 35128 Padua, Italy; alessandra.biffi@unipd.it
* Correspondence: d.corallo@irpcds.org
† These authors contributed equally to this work.

Abstract: Neuroblastoma, the most common pediatric extracranial solid tumor, arises from the malignant transformation of neural crest progenitors in the peripheral nervous system. Its clinical and genetic heterogeneity poses significant challenges, especially in high-risk patients with metastatic disease. Two plastic neuroblastoma cell phenotypes, adrenergic (ADR) and mesenchymal (MES), have been identified. Notably, MES neuroblastoma cells exhibit increased migration and chemoresistance. Cancer-associated fibroblasts (CAFs) in the tumor microenvironment further promote tumor aggressiveness by enhancing cancer cell proliferation, extracellular matrix remodeling, angiogenesis and metastasis. This study explored the role of non-activated fibroblasts in ADR and MES neuroblastoma cell proliferation, migration and invasion in vitro and in vivo. Results showed that MES and ADR neuroblastoma cells influenced fibroblast activation into CAFs differently, with MES cells promoting a more invasive environment leading to tumor spread. These findings enhance our understanding of how ADR and MES phenotypes contribute to the formation of a pro-metastatic niche by activating fibroblasts in CAFs. This insight could inform new therapeutic strategies targeting the tumor microenvironment to prevent neuroblastoma metastasis.

Keywords: cancer-associated fibroblast (CAF); neuroblastoma; metastasis; cell migration; tumor microenvironment; cancer dissemination

check for updates

Citation: Corallo, D.; Nardelli, C.; Pantile, M.; Menegazzo, S.; Biffi, A.; Aveic, S. Exploring the Role of Fibroblasts in Promoting Neuroblastoma Cell Migration and Invasion. *J. Nanotheranostics* **2024**, *5*, 212–227. https://doi.org/10.3390/jnt5040013

Academic Editors: Seyed Moein Moghimi and Dmitri Simberg

Received: 24 September 2024
Revised: 15 November 2024
Accepted: 6 December 2024
Published: 8 December 2024

Copyright: © 2024 by the authors. Licensee MDPI, Basel, Switzerland. This article is an open access article distributed under the terms and conditions of the Creative Commons Attribution (CC BY) license (https://creativecommons.org/licenses/by/4.0/).

1. Introduction

Neuroblastoma is the most common extracranial solid tumor of infancy that originates from the malignant transformation of the neural crest of the sympathetic nervous system [1,2].

The intra- and inter-tumor heterogeneity that characterizes neuroblastoma is one of the most limiting features for the successful treatment of the disease. In particular, neuroblastoma cells have been categorized into two predominant epigenetically regulated cell phenotypes, named adrenergic (ADR) and mesenchymal (MES) [3,4]. While the ADR neuroblastoma cells display a neuroplastic phenotype characterized by a gene signature involved in the sympatho-adrenergic differentiation, the MES cells appear undifferentiated and more similar to their neural crest progenitors. In addition, MES neuroblastoma cells express several MES markers that favor their migration and chemoresistance [3,4]. The ability of neuroblastoma cells to switch from one phenotype to the other makes the development of effective treatments for neuroblastoma patients challenging.

More recently, the global description of the tumor microenvironment (TME) by single-cell transcriptomics provided a more comprehensive dissection of the cellular heterogeneity composing neuroblastomas. In this context, the TME has received increasing interest in the development of innovative and personalized anti-cancer strategies [5]. To this end,

the role of immune cells in neuroblastoma has been extensively studied and a strong correlation between the epigenetic status of neuroblastoma cells and immunogenicity has been established [6,7]. However, the reciprocal interaction between the ADR and MES neuroblastoma cells and the non-immune components of the TME remains to be fully characterized.

Cancer-associated fibroblasts (CAFs) represent a major component of TME in solid tumors. The CAFs are a heterogeneous group of cells that arise not only from the activation of resident fibroblasts but also from other stromal cell populations, such as epithelial cells and mesenchymal stem cells [8,9]. Once activated, CAFs acquire myofibroblast properties including de novo synthesis of the alpha-smooth muscle actin (α-SMA) protein [10,11]. Single-cell analysis of neuroblastoma tumors has revealed two distinct CAF subtypes: CAF-S1, which displays immunosuppressive functions and CAF-S4, which exhibits pro-metastatic functions [12–14]. CAFs interact dynamically with cancer cells through different mechanisms including direct contacts and paracrine secretion of growth factors, inflammatory cytokines and chemokines [15,16]. Additionally, CAFs regulate extracellular matrix deposition and organization [17,18]. In neuroblastoma, CAFs have been shown to support malignant cell proliferation [19], drive tumor angiogenesis [20], induce immunosuppression by interacting with tumor-associated macrophages and contribute to neuroblastoma chemoresistance [21,22]. Despite this clear evidence of CAFs' role in influencing neuroblastoma growth, survival and invasiveness, the reciprocal interaction between CAFs and MES or ADR neuroblastoma cells in the primary tumor niche needs to be fully clarified.

In this study, we performed in vitro and in vivo assays to explore the role of non-activated fibroblasts in promoting proliferation, migration and invasion of several ADR or MES neuroblastoma cells. Our data revealed that the phenotype of neuroblastoma cells differentially influences the transformation of fibroblasts into CAFs by direct cell–cell contact. We found that MES neuroblastoma cells promote the proliferation and activation of fibroblasts into CAFs. In turn, CAFs secrete extracellular matrix (ECM) proteins and create a pro-invasive environment to support cancer cell dissemination. Our findings extended the understanding of how the ADR and MES phenotypes differentially influence the interaction between neuroblastoma cells and fibroblasts. In particular, we demonstrated that MES neuroblastoma cells take advantage of the fibroblasts to create a pro-metastatic environment for enhanced tumor cell dissemination. This evidence underscores the importance of considering the complexity of the TME as a function of neuroblastoma cell phenotypic heterogeneity to design optimized strategies against metastatic disease.

2. Materials and Methods

Cell cultures. Human neuroblastoma IMR-32 and SH-SY5Y cell lines were selected as ADR neuroblastoma cell lines. SK-N-AS cell line was selected as the MES neuroblastoma cell line [4]. Cells were cultured in RPMI-1640 medium (Sigma-Aldrich, St. Louis, MO, USA) supplemented with 2 μM L-Glutamine (Gibco, Thermo Fisher Scientific, Waltham, MA, USA) and 10% Fetal Bovine Serum (FBS) (Gibco, Thermo Fisher Scientific, Waltham, MA, USA), 1% Penicillin/Streptomycin/Amphotericin B Solution (Sartorius, Gottingen, Germany) and maintained at 37 °C, 5% CO_2 and 95% humidity.

The adrenergic 691-ADR and mesenchymal 691-MES neuroblastoma cell lines (kind gift of Prof. Dr. Jan Molenaar, Utrecht University) were described previously [23] and cultured in 1:1 mixture of DMEM/F12 medium (Sigma-Aldrich, St. Louis, MO, USA) supplemented with 10 μg/mL fibroblast growth factor (FGF) (Gibco, Thermo Fisher Scientific, Waltham, MA, USA), 10 μg/mL epithelial growth factor (EGF) (Gibco, Thermo Fisher Scientific, Waltham, MA, USA), 1X N2 and B27 (Gibco, Thermo Fisher Scientific, Waltham, MA, USA), 1% Penicillin/Streptomycin (Gibco, Thermo Fisher Scientific, Waltham, MA, USA) at 37 °C, 5% CO_2 and 95% humidity. Human BJ fibroblasts cell line (ATCC, Manassas, VA, USA) was maintained in a 1:1 mixture of DMEM/F12 medium (Sigma-Aldrich, St. Louis, MO, USA) supplemented with 2 μM Glutamine (Gibco, Thermo Fisher Scientific, Waltham, MA, USA), 1% Penicillin/Streptomycin/Amphotericin B Solution (Sartorius, Gottingen,

Germany), 2% fetal bovine serum (FBS) (Gibco, Thermo Fisher Scientific, Waltham, MA, USA) at 37 °C with 5% CO_2 and 95% humidity.

Direct 2D co-cultures. Pre-staining with either 500 nM CellTraceTM CFSE (Invitrogen, Thermo Fisher Scientific, Waltham, MA, USA) at 37 °C for 10 min or Vybrant™ Multicolor Cell-Labeling Kit (Invitrogen, Thermo Fisher Scientific, Waltham, MA, USA) for 20 min at 37 °C was performed to distinguish between neuroblastoma cell lines and BJ fibroblasts, as reported in the figure legends. Single-cell suspensions of SK-N-AS (8×10^4 cells), IMR-32 (2.5×10^5 cells) or SH-SY5Y (2×10^5 cells) were mixed at a 4:1 ratio with BJ fibroblasts in supplemented RPMI-1640 medium on a 6-well plate with glass coverslips. Single-cell suspension of 691-ADR and 691-MES (2×10^5 cells) was mixed at a 4:1 ratio with BJ fibroblasts in supplemented DMEM/F12. After 6 days of co-culture, the cells were fixed with 4% PFA solution and stored at 4 °C for immunofluorescence staining.

Transwell 2D co-cultures. BJ fibroblasts (2×10^5) were seeded onto a 24-well plate (lower chamber) with glass coverslips. Neuroblastoma cells (5×10^5) were seeded onto the upper chamber of a transwell (Corning, NY, USA) with a membrane pore size of 0.4 μm. Cells were incubated for 6 days and then fixed with 4% PFA solution and stored at 4 °C for α-SMA immunofluorescence staining.

Generation and cryosectioning of three-dimensional multicellular tumor spheroids (MCTSs). Single-cell suspensions of 2×10^4 (SK-N-AS and SH-SY5Y) or 4×10^4 (IMR-32) neuroblastoma cells were mixed at a 4:1 ratio with pre-labeled Vybrant-DiO BJ fibroblasts seeded in a 96-well ultra-low adhesion (ULA) plate (Nunclon Sphera 96 U Bottom Plate, Thermo Fisher, Waltham, MA, USA). The same number of unmixed neuroblastoma cells and BJ fibroblasts were used as controls. To induce cell aggregation, the plate was centrifuged at $300\times g$ for 3 min and incubated at 37 °C with 5% CO_2 and 95% humidity. Mono- and co-culture growth kinetics were evaluated daily for up to 6 days. At least 12 MCTSs were generated and analyzed for each co-culture condition. The Axio Observer 7 microscope, Jena, Germany) was used to monitor the localization of BJ fibroblasts within the spheroids for 6 days.

For MCTS invasion and immunofluorescence assays, neuroblastoma and BJ cells were pre-labeled with Vybrant CM-DiD (Invitrogen, Thermo Fisher Scientific, Waltham, MA, USA) following the manufacturer's instruction. The MCTSs grown for 6 days were fixed in 4% PFA solution at room temperature for 2 h. The MCTSs were then incubated overnight at 4 °C in 30% sucrose and progressively frozen in OCT using isopentane vapor and liquid nitrogen. 15 μm-thick slices were obtained with a Cryostat Leica CM1950.

Viability assay on MCTSs. The viability of MCTSs was assessed through a Live/Dead assay (Molecular Probes, Invitrogen, Thermo Fisher Scientific, Waltham, MA, USA). Briefly, 6 days monoculture spheroids and MCTSs were stained with a solution of 2 μM calcein AM and 4 μM ethidium homodimer-1 for 30 min at 37 °C. Then, they were fixed in 4% PFA solution and imaged with an LSM800 confocal microscope (Zeiss, Jena, Germany). Nuclei were counterstained with Hoechst-33342 (Sigma Aldrich, St. Loius, MO, USA). Cell viability was measured using Fiji software (National Institutes of Health, Bethesda, MD, USA).

In vitro wound-healing assay. DiD-labeled single-cell suspension of neuroblastoma cells was mixed at a 4:1 ratio with DiO-labeled fibroblasts in RPMI complete medium for 6 days. Single-cell suspensions of unmixed neuroblastoma and BJ cells were used as controls. The cells were transferred onto a 2-well Culture-Insert (Ibidi, Gräfelfing, Germany) to create a uniform wound and incubated at 37 °C, 5% CO_2 and 95% humidity for 24 h. After that, the silicon insert was removed and the cells were grown in RPMI-1640 medium supplemented with 2% FBS. Migration of mono- and co-culture cells was daily monitored, and images were captured using an Axio Observer 7 inverted fluorescence microscope (Zeiss) at 0, 24 and 48 h after wounding. The quantification of the scratched area was obtained using Fiji software, version 2.14.0 (National Institutes of Health, Bethesda, MD, USA).

Matrigel cell invasion assay. The monoculture spheroids and MCTSs were embedded in a solution of 50% Matrigel (Corning, NY, USA) and daily imaged up to 7 days using an

Axio Observer 7 inverted fluorescence microscope (Zeiss, Jena, Germany). The invaded area (mm^2) of tumor spheroids was analyzed using Fiji software, version 2.14.0 (National Institutes of Health, Bethesda, MD, USA).

Immunofluorescence. Immunofluorescence on MCTSs was performed by permeabilizing the cryosections with 0.3% Triton X-100 (Sigma-Aldrich, St. Louis, MO, USA) diluted in PBS for 30 min at room temperature. Slices were then blocked in 5% goat serum (Merk Millipore, Burlington, MA, USA) for 1 h at room temperature and incubated with the primary antibodies in 2.5% goat serum (Merk Millipore, Burlington, MA, USA) overnight at 4 °C. The slices were then washed three times with PBS and incubated with secondary antibodies in 2.5% goat serum for 1 h. Nuclei were counterstained with DAPI (Invitrogen, Thermo Fisher Scientific, Waltham, MA, USA). Finally, the slices were mounted on glass coverslips and imaged using a Zeiss LSM 800 confocal microscope. Images were processed using Fiji software, version 2.14.0 (National Institutes of Health, Bethesda, MD, USA).

For immunofluorescence on 2D cell culture, cells were permeabilized in 0.1% Triton X-100 for 15 min at room temperature and blocked in 5% goat serum (Merk Millipore, Burlington, MA, USA) for 45 min. Cells were incubated overnight with primary antibodies diluted in 2.5% goat serum (Merk Millipore, Burlington, MA, USA). After three washes, the cells were stained with secondary antibodies in 2.5% goat serum (Merk Millipore, Burlington, MA, USA) for 45 minutes. Finally, the samples were observed through a Zeiss LSM 800 confocal microscope. The quantification of CAFs and proliferating cells was obtained with Fiji software, version 2.14.0 (National Institutes of Health, Bethesda, MD, USA). Primary and secondary antibodies are listed in Table 1.

Table 1. List of primary and secondary antibodies.

Antibodies	Species	Dilution	Source	Catalog Number
Alpha-smooth muscle Actin	Mouse IgG2a	1:1000	Abcam	AB7817
FAP	Rabbit IgG (H + L)	1:100	Arigo biolaboratories	ARG66701
NCAM	Rabbit	1:100	Novus	NBP2-66968
GD2	Mouse IgG2a	1:200	Santa Cruz	SC-53831
Ki-67	Mouse	1:50	Santa Cruz	SC-23900
COL1A1	Rabbit	1:100	Novus	NB600-408
COL4A1	Goat	1:400	Novus	NBP1-26549
LAM-89	Mouse	1:100	Novus	NB600-883
AlexaFluor 546	Mouse IgG2a (γ2a)	1:1000	Invitrogen	A21133
AlexaFluor 633	Rabbit IgG (H + L)	1:1000	Invitrogen	A21070
AlexaFluor 594	Goat IgG (H + L)	1:1000	Invitrogen	A11058
AlexaFluor 488	Anti-Rabbit IgG (H + L)	1:1000	Invitrogen	A32731

Zebrafish embryo preparation and xenotransplantation. For xenotransplantation experiment [24] DiL-labeled neuroblastoma cells and DiO-labeled fibroblasts were co-cultured for 6 days of co-culture. Then, 1×10^6 cells were resuspended in 10 µL PBS before the injection. Wild-type AB zebrafish embryos were dechorionized and anesthetized at 48 h post fertilization (hpf) with 0.003% tricaine (Sigma-Aldrich, St. Louis, MO, USA). Approximately 200 cells were injected into the perivitelline space of each embryo, using borosilicate glass capillary needles (OD/ID: 1.0/0.75 mm, WPI), a Pneumatic Picopump and a micromanipulator (WPI). Following implantation, zebrafish embryos were kept at 34 °C and examined 2 h post-injection (hpi). This screening process aimed to exclude from further analysis any embryo that was damaged, had human cells present in the bloodstream or exhibited fluorescence loss related to engrafted cells. For this reason, IMR-32 (ADR type) and SK-N-AS (MES type) neuroblastoma cells were selected for the

xenotransplantation experiments, as they showed the highest engraftment success in zebrafish embryos, minimizing cell loss associated with lower grafting capability. Tumor invasion events were captured at 24 hpi and imaged using an Axio Observer 7 microscope (Zeiss, Jena, Germany). Quantification of disseminated cells was manually performed.

Statistical Analysis. Results were presented as mean ± SEM (standard error of the mean). All the experiments were repeated at least three times. Statistical analyses were performed using GraphPad Prism 10 (GraphPad, La Jolla, CA, USA). Statistical significance was determined by an unpaired two-tailed t-test or two-way ANOVA followed by the post hoc Fisher's LSD test (* $p < 0.05$, ** $p < 0.01$, *** $p < 0.001$).

3. Results

The ADR and MES neuroblastoma cells differently interact with fibroblasts to form multicellular tumor spheroids. To study the tumor–fibroblast interaction, we generated MCTSs by combining ADR and MES neuroblastoma cells with fibroblasts in 96-well ultra-low-adhesion plates. This setup allowed us to compare the growth kinetics of MCTSs with their respective neuroblastoma spheroid monocultures. We first noticed that the formation of IMR-32 spheroids monoculture required higher seeding density (4×10^4) compared to the other neuroblastoma cell lines investigated. All the MCTSs exhibited similar growth kinetics compared to their corresponding monocultures (Figure 1A). Only IMR-32 cells co-cultured with fibroblasts showed a significantly faster aggregation (p-value < 0.01) within the first 24 h (Figure 1A). However, once aggregated, the IMR-32 spheroids and the corresponding MCTSs became similar in dimension and maintained comparable growth kinetics over time (Figure 1A). Together with similar growth kinetics, comparable viability with no significant differences was recorded between paired monoculture spheroids and MCTSs, including IMR-32 mono- and co-cultures at day 1 (Figures 1B and S1). Next, we monitored the arrangement of fibroblasts within MCTSs over time. When mixed with MES SK-N-AS neuroblastoma cells, fibroblasts were located scattered throughout the spheroid (Figure 1C). In the presence of the ADR neuroblastoma cell lines (IMR-32 and SH-SY5Y), we observed a core-shell structure where fibroblasts localized centrally within the spheroid core and the neuroblastoma cells located externally. Consequently, the MCTSs allowed to dissect the differential interaction of fibroblasts with ADR and MES neuroblastoma cells.

The co-culture of MES neuroblastoma cells and fibroblasts induces extracellular matrix deposition. We then investigated whether the secretion of the ECM essential for the establishment of the metastatic niche might be differently influenced by neuroblastoma cells.

Thus, we evaluated the expression of collagen alpha-1(IV) chain (COL4A1), collagen alpha-1(I) chain (COL1A1) and laminin as three abundant ECM components of the adrenal gland, the most common primary site of neuroblastoma [25]. Immunofluorescence analysis revealed that fibroblasts in monoculture did not secrete COL4A1. However, in co-culture with SK-N-AS cells, strong COL4A1 deposition was localized to the core of MCTSs, where most of the fibroblasts localized, forming an extensive extracellular network throughout the MCTS (Figure 2A). In contrast, only a slight or absent deposition of COL4A1 was observed in the ADR IMR-32 and SH-SY5Y MCTSs. Notably, the deposition of COL1A1 was also more pronounced in the MES MCTSs than in the ADR MCTSs (Figure 2B). When looking at laminin, the localization drastically changed in MES MCTSs compared to fibroblast monoculture. Indeed, while the fibroblasts showed a diffuse cytoplasmic staining, in the MES MCTSs laminin appeared differentially organized in a net-like structure (Figure 2C). Again, the ADR MCTSs did not secrete laminin. These data indicated that MES and ADR neuroblastoma cell lines differentially affect the secretion and organization of the ECM. In particular, the interaction between MES neuroblastoma cells and fibroblasts strongly increases the secretion and deposition of COL4A1 and laminin.

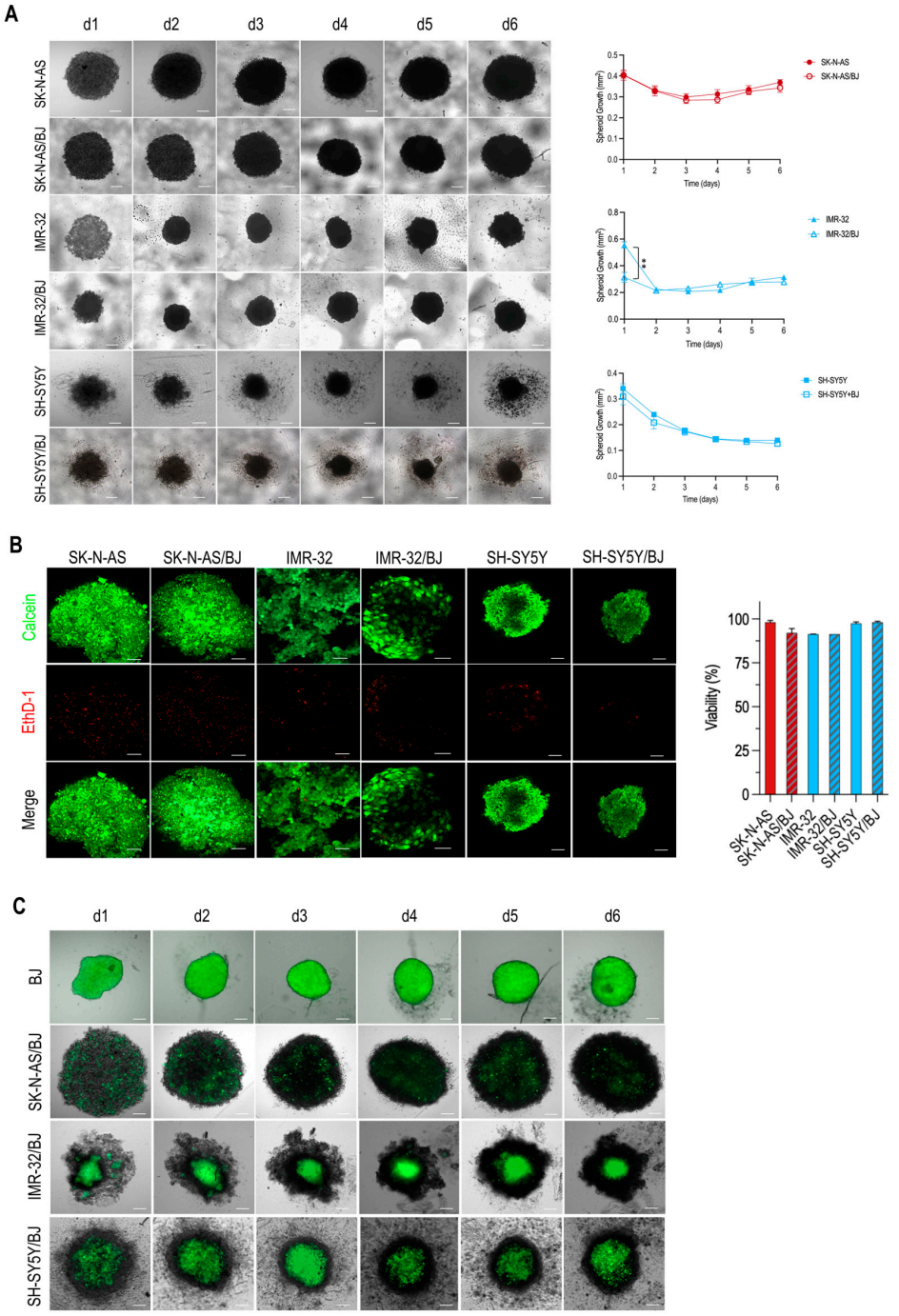

Figure 1. Generation of multicellular tumor spheroids (MCTSs) to study the interaction between adrenergic (ADR) and mesenchymal (MES) neuroblastoma cells with fibroblasts. (**A**) Representative brightfield images of monoculture spheroids and MCTSs generated from SK-N-AS, IMR-32 and SH-SY5Y with BJ fibroblasts cultured for 6 days. Scale bars: 200 µm. The quantification of the spheroid growth area (mm^2) was reported on the right. Data were presented as mean ± SEM, $n = 3$, ** $p < 0.01$. (**B**) Representative Z-stack fluorescence images of monoculture spheroids and MCTSs viability (%) at 6 days of culture. MCTSs were stained with Calcein (green, live cells) and EthD-1 (red, dead cells). Scale bars: 200 µm. The mean percentage (%) of viable cells was represented in the histogram on the right. Statistical analysis was performed between MCTS and the respective NB monoculture. Data were presented as mean ± SEM, n = 3 (**C**) Representative fluorescence images of BJ fibroblast localization into monoculture spheroids and MCTSs with the indicated neuroblastoma cells over time (days, d). BJ fibroblasts were pre-labeled with Vybrant-DiO (green). Scale bars: 200 µm.

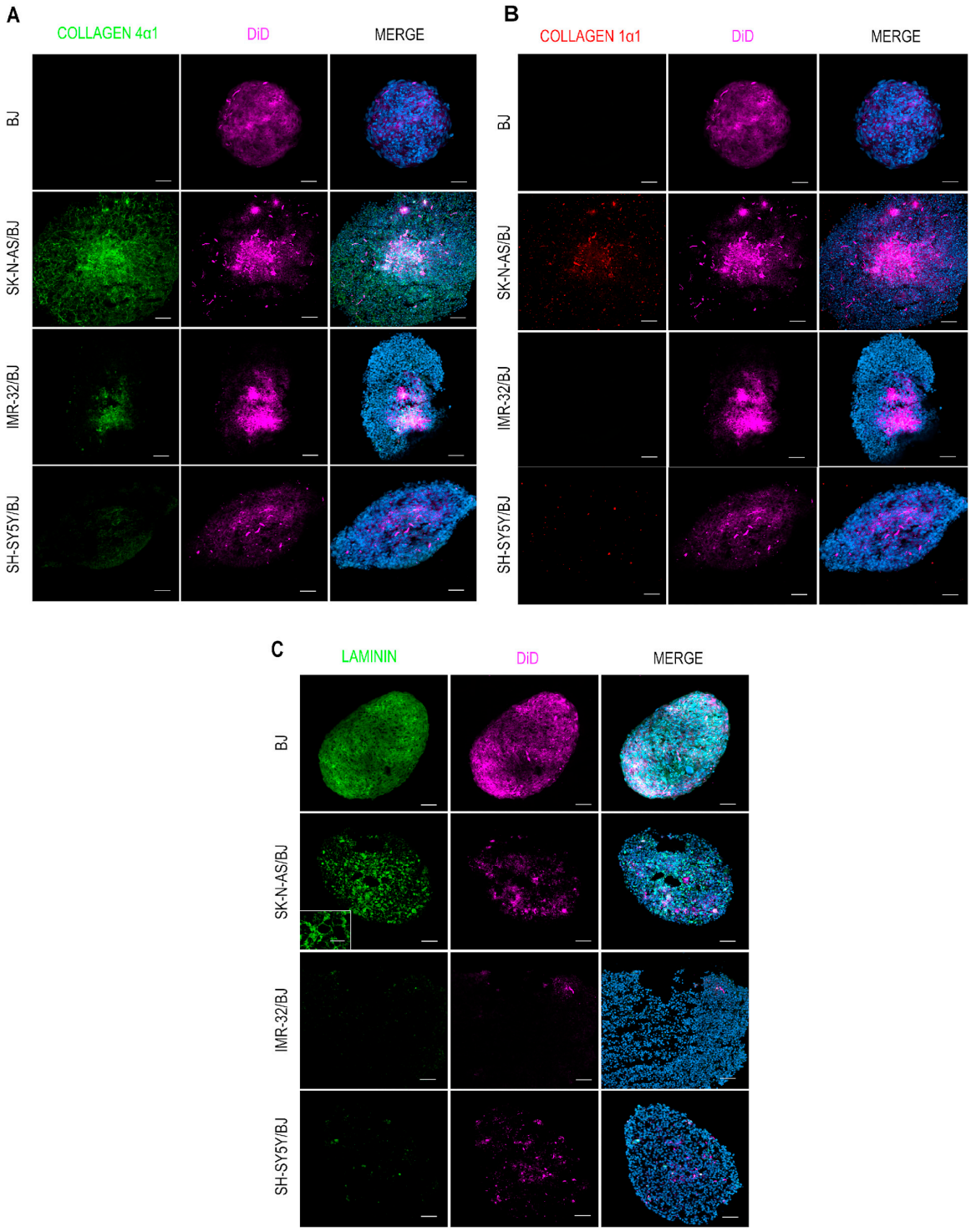

Figure 2. The co-culture of MES neuroblastoma cells with fibroblasts induced the secretion of extracellular matrix (ECM) proteins. Representative images of immunofluorescence staining of 15 µm-thick slices from SK-N-AS, IMR-32, SH-SY5Y MCTSs for (**A**) Collagen 4-α1 (green), (**B**) Collagen 1-α1 (red) and (**C**) Laminin (green). BJ fibroblasts were pre-labeled with Vybrant-DiD (purple) while nuclei were stained with DAPI (blue). Scale bars: 50 µm. The white box showed the magnification of laminin deposition in SK-N-AS MCTS. Scale bar: 5 µm.

Neuroblastoma cells induced the transformation of fibroblasts into cancer-associated fibroblasts. Given the well-established association between increased ECM deposition and the presence of CAFs in the tumor microenvironment [26], we investigated whether the

presence of neuroblastoma cells could induce the activation of fibroblasts into CAFs in the MCTSs. Immunofluorescence staining for alpha-smooth muscle actin (α-SMA) revealed a positive signal in all the MCTSs compared to fibroblasts monoculture (Figure 3A). We then used a 3D co-culture model to better characterize the subcellular localization of α-SMA. About 80% of fibroblasts expressed α-SMA protein accumulated in stress fibers after six days of co-culture with the MES SK-N-AS cells (Figure 3B). This effect was observed to a significantly lesser extent in BJ co-cultured with ADR IMR-32 and SH-SY5Y cells. In contrast, BJ monocultures had almost undetected α-SMA expression, not localized in stress fibers (Figure 3B). The transformation of BJ into CAFs only in MES cell co-cultures was also confirmed through FAP [27,28] staining (Figure S2).

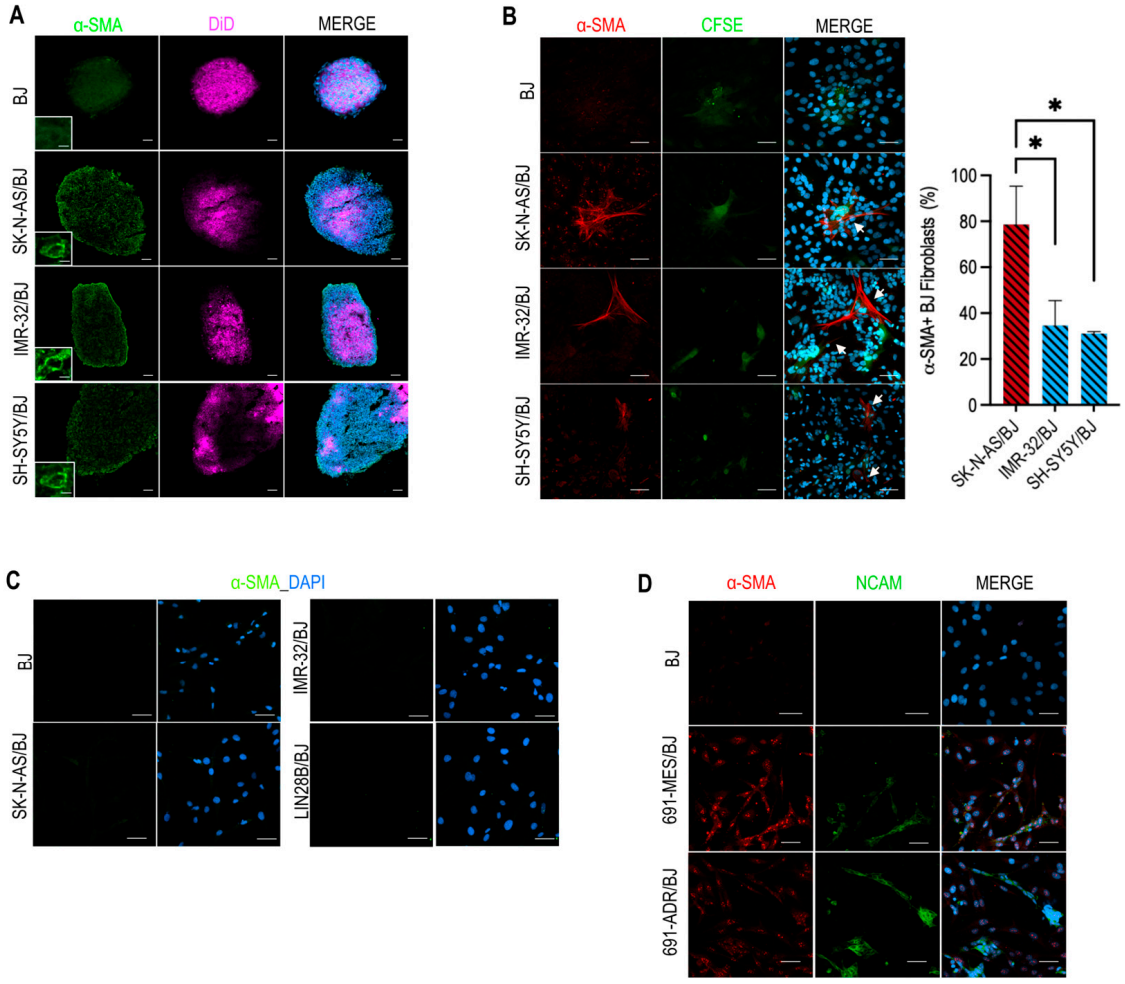

Figure 3. The direct cell–cell contact of neuroblastoma cells and fibroblasts induced CAF activation. (**A**) Representative images of immunofluorescence staining for α-SMA (green) on BJ, SK-N-AS, IMR-32, SH-SY5Y MCTSs. BJ fibroblasts were pre-labeled with Vybrant-DiD (purple) and the nuclei were stained with DAPI (blue). Scale bars: 50 μm. White boxes showed a magnification of the staining. Scale bars: 5 μm. (**B**) The α-SMA immunostaining (red) on the indicated mono- and co-cultures. BJ cells were labeled with CFSE (green), whereas nuclei were stained with DAPI (blue). White arrows indicated the α-SMA staining in CAFs. Scale bars: 50 μm. Statistical analysis was conducted between the MCTS. Data were presented as mean ± SEM, n = 4, * $p < 0.05$. (**C**) Immunostaining for α-SMA (green) on BJ fibroblasts of a transwell assay with the indicated neuroblastoma cells. Nuclei were stained with DAPI (blue). Scale bars: 50 μm. (**D**) Representative images of immunofluorescence staining for α-SMA in 691-MES and 691-ADR neuroblastoma cells co-cultured with BJ fibroblasts. Neuroblastoma cells were stained with NCAM (CD56; green), while nuclei were stained with DAPI (blue). BJ monocultures were used as controls. Scale bars: 50 μm.

Furthermore, α-SMA deposition into stress fibers was not detected when the two cell populations were grown into separate chambers (Figure 3C), suggesting that paracrine signals were not the main drivers of CAF transformation. Consequently, direct cell–cell contact is required to induce the activation of CAFs under the tested culture conditions. We further validated this observation by using the 691-ADR and 691-MES neuroblastoma cells [3,24]. Notably, 691-MES neuroblastoma cells induced enhanced α-SMA and FAP expression in co-cultured fibroblasts compared to 691-ADR cells (Figures 3D and S2). Nevertheless, α-SMA did not localize in stress fibers but accumulated in the nucleus and cytoplasm of activated fibroblasts (Figure 3D). Overall, these results indicated that the MES phenotype of neuroblastoma cells enhanced their ability to activate fibroblasts into CAFs through direct cell–cell contact.

The MES neuroblastoma cells enhanced the proliferation of fibroblasts. Next, we examined the reciprocal influence of fibroblasts and neuroblastoma cells on the proliferation of both populations through Ki-67 immunostaining. Although not significant, we observed a tendency towards increased proliferation of neuroblastoma cells in all ADR and MES co-cultures, compared to the monocultures. Differently, we observed that fibroblast proliferation significantly doubled when co-cultured with MES SK-N-AS neuroblastoma cells compared to the fibroblast monoculture and to the ADR co-cultures (Figure 4A). As for the previous cellular setting, the proliferation of 691-MES and 691-ADR neuroblastoma cells was not affected by the co-culture with fibroblasts (Figure 4B). However, the proliferation of fibroblasts was significantly enhanced in the presence of 691-MES cells compared to the 691-ADR/BJ co-culture (Figure 4B). This result was consistent with what was observed with the SK-N-AS cell line, confirming that only the MES neuroblastoma cells significantly induced fibroblast proliferation.

Fibroblasts promoted MES neuroblastoma cell invasiveness in vitro and metastasis in vivo. To investigate the role of activated fibroblasts in the migration and invasion of ADR and MES neuroblastoma cells, we conducted cell migration and invasion assays. Fibroblasts did not affect ADR IMR-32 and MES SK-N-AS migration but enhanced SH-SY5Y migration, closing the wound site 24 h earlier in co-culture compared to monoculture (Figure S3). By examining the invasion, only the MES SK-N-AS significantly spread outside the spheroids and invaded the ECM faster in MCTSs compared to monoculture (Figure 5A). In particular, fibroblasts were the first to extend beyond the spheroid, supporting SK-N-AS cell migration over their invasive edge (Figure 5A). Conversely, the invasion of ADR SH-SY5Y cells was significantly inhibited in the presence of fibroblasts, while IMR-32 cells' inability to invade the extracellular matrix remained unchanged (Figure 5A). In line with these results, the co-culture of 691-MES neuroblastoma cells, but not 691-ADR, showed enhanced invasive phenotype in MCTSs compared to monoculture (Figure 5B). Thus, these results suggest that the presence of activated fibroblasts markedly promoted the invasion of MES neuroblastoma cells. To validate these findings, we took advantage of an in vivo zebrafish model in which co-cultures (and their corresponding tumor monoculture as a control) were engrafted into the perivitelline space of 48-hpf embryos. The number of disseminated cells found located in the posterior region of each animal after 24 h was recorded (Figure 5C, left). We found that the injection of the MES SK-N-AS/BJ co-culture led to a marked increase in the number of disseminated cells, both neuroblastoma and fibroblasts (Figure 5C). In contrast, engrafted mono- and co-culture of ADR IMR-32 could not disseminate in the zebrafish tail, thus confirming the results obtained in vitro (Figure 5C). Together, these findings demonstrated that CAFs facilitate MES neuroblastoma cell invasion in vitro and metastatic dissemination in vivo.

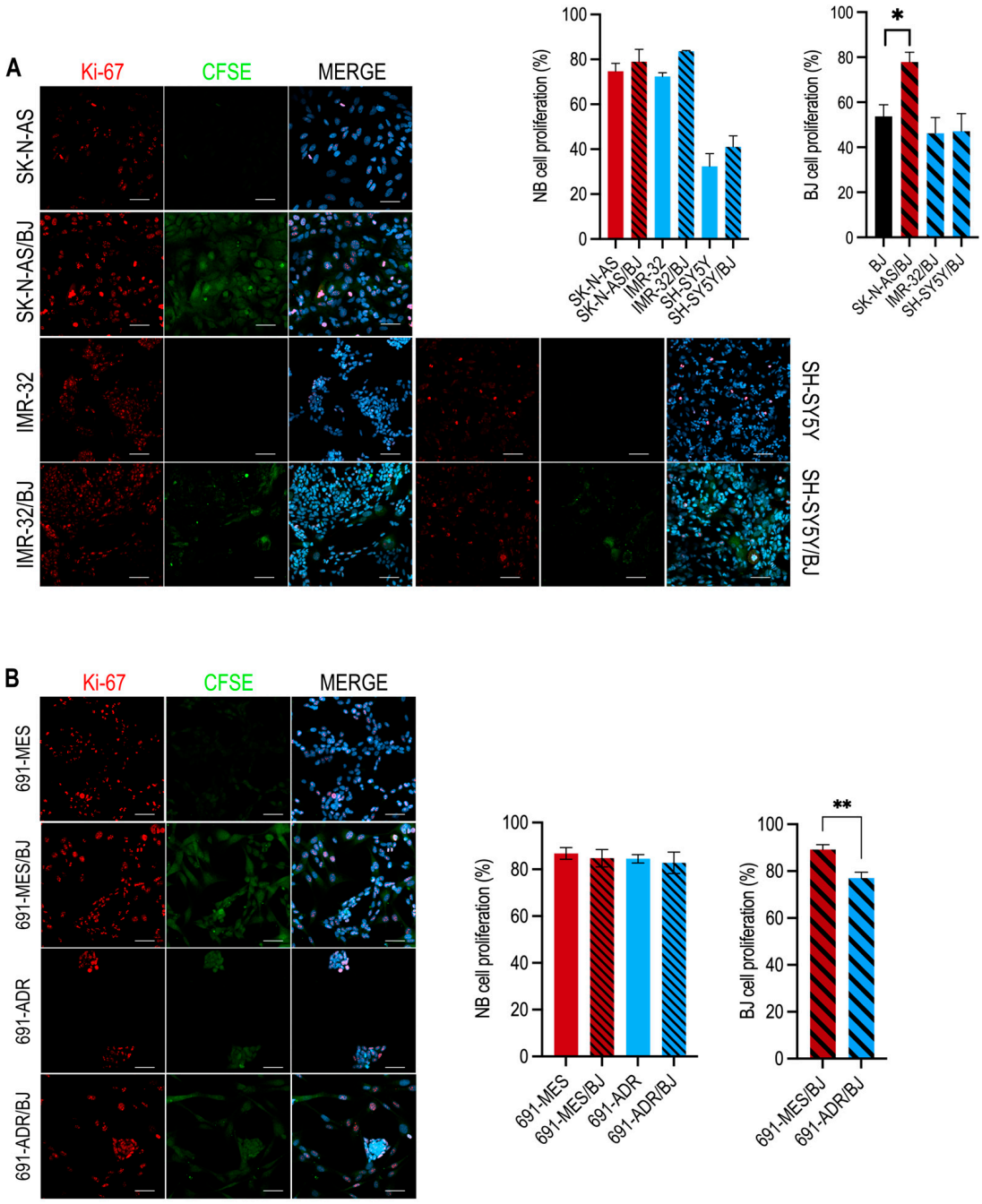

Figure 4. The co-culture of fibroblasts with MES neuroblastoma cells enhanced fibroblast proliferation. (**A**) Immunofluorescence staining for Ki67 (red) in monoculture and MCTSs of SK-N-AS, IMR-32, and SH-SY5Y neuroblastoma cells with BJ fibroblasts, pre-labeled with CFSE (green). Nuclei were stained with DAPI (blue). Scale bars: 50 µm. Quantification of Ki67-positive cells counted from 10 random fields was reported in the adjacent histograms. Statistical analysis was performed between the MCTS and the relative NB and BJ monoculture. Data were presented as mean ± SEM, n = 4 * $p < 0.05$. (**B**) Immunofluorescence staining for Ki67 (red) in monoculture and MCTSs of 691-MES and 691-ADR neuroblastoma cells with BJ fibroblasts pre-labeled with CellTracer CFSE (green). Nuclei were stained with DAPI (blue). Scale bars: 50 µm. Quantification of Ki67-positive cells counted from 6 random fields was presented in the histograms on the right. In the NB cell-proliferation analysis, the comparisons were made between the MCTS and the corresponding NB monoculture, while in the analysis of BJ cell proliferation, the comparisons were conducted among the different MCTS groups. Data were presented as mean ± SEM, n = 3 ** $p < 0.01$.

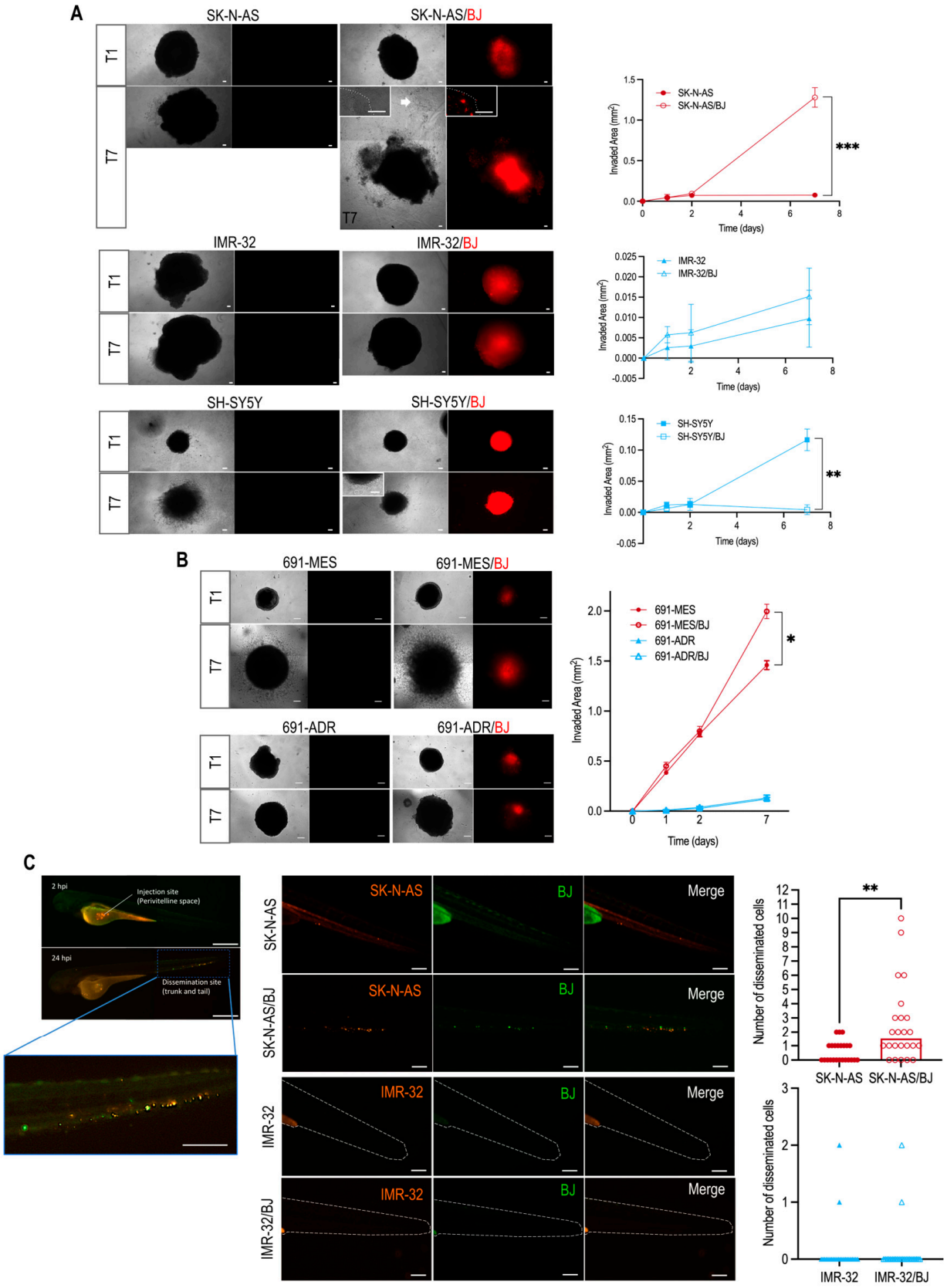

Figure 5. Fibroblasts supported MES neuroblastoma cells invasiveness in vitro and metastasis in vivo. (**A**) Representative fluorescence images of control spheroids and MCTSs after 6 days of co-culture embedded in Matrigel. BJ cells were pre-labeled with Vybrant-DiD (red). Spheroids were monitored

at day 1 (T1) and 7 days (T7). Scale bars: 200 µm. White boxes showed higher magnifications of the invasive front of disseminated SK-N-AS neuroblastoma cells (indicated with the white arrow). Scale bars: 5 µm. The invading cell area was manually calculated for each time point (days) and reported in the graphs on the right. Statistical analysis was conducted between the MCTS and the respective NB monoculture. Data were presented as mean ± SEM, n = 6, ** $p < 0.01$, *** $p < 0.001$. (**B**) Representative fluorescence images of 691-MES and 691-ADR control spheroids and MCTSs with BJ fibroblasts after 7 days in Matrigel. BJ fibroblasts were pre-labeled with Vybrant-DiD (red). Scale bars: 200 µm. Statistical analysis was conducted between the MCTS and the respective NB monoculture. Data were presented as mean ± SEM, n = 6 * $p < 0.05$. (**C**) Representative lateral views of a zebrafish xenotransplanted embryo at 2 h post-injection (hpi, top) and 24 hpi (bottom), showing the injection site in the perivitelline space and in the metastatic site of the caudal region (dotted blue square with magnification below). Live-fluorescent microscopy images of the trunk region of 24 hpi zebrafish embryos injected with mono- and co-culture of SK-N-AS and IMR-32 cells with BJ fibroblasts. Neuroblastoma cells were pre-labeled with Vybrant-DiL (orange) while BJ cells were labeled with Vybrant-DiO (green). Dotted lines highlighted the trunk and tail regions of xenotransplanted embryos. Scale bar: 200 µm. The number of disseminated cells was manually quantified. Each dot represents the number of disseminated cells from a single embryo. Statistical analysis was conducted between the MCTS and the respective NB monoculture. Data were presented as mean ± SEM, n = 23, * $p < 0.01$.

4. Discussion

Metastasis is the predominant cause of mortality in neuroblastoma patients [29,30]. Therefore, understating the molecular mechanisms that drive cancer cell dissemination is an urgent need for the development of effective therapeutic strategies. Our study provided new insights into how neuroblastoma cells exploit the TME to enhance their metastatic potential, with CAF playing a key role in this process.

We generated MCTSs to investigate the interaction between non-activating fibroblasts and neuroblastoma cells selected based on their ADR and MES phenotypes [4]. We demonstrated that MES neuroblastoma cells possess enhanced capability to activate fibroblasts in CAFs compared to the ADR neuroblastoma cells. Although TGF-β is recognized as the most potent paracrine signaling molecule involved in CAF activation and α-SMA expression [31–33], our study demonstrated that paracrine signals alone were insufficient for neuroblastoma cells to induce fibroblast activation within 6 days, whereas direct cell-to-cell contact between these cell populations was essential to observe α-SMA expression. Nevertheless, paracrine signaling may contribute to the differential activation of CAFs observed in co-cultures with ADR and MES neuroblastoma cells in a time-dependent manner. In this context, Proestler et al. demonstrated that neuroblastoma cells influence the activation of fibroblasts by secreting extracellular vesicles containing miR-574-5p which modulates α-SMA expression through TLR7/8 signaling pathway [34].

Regarding its subcellular localization, we observed that α-SMA protein was deposited predominantly in stress fibers. The accumulation of α-SMA within these microfilament bundles is known to enhance CAF contractility and alter the ECM composition through mechanical stimuli and paracrine factors [35–38]. Interestingly, when fibroblasts were co-cultured with 691-MES and 691-ADR neuroblastoma cell lines did not lead to α-SMA-positive stress fiber polymerization, but instead to the accumulation of the protein into the cytoplasm and nucleus of fibroblasts. In general, we observed that the neuroblastoma MES phenotype was responsible for α-SMA protein expression but not its subcellular localization in CAFs, suggesting that other mechanisms are responsible for regulating α-SMA localization. Other studies have demonstrated significant heterogeneity in the levels of αSMA protein in CAFs in other pathological conditions, such as oral tumors [39] and fibrosis [40]. However, no data dissecting this phenotype in patient-derived neuroblastoma samples or in vitro have been reported. The mechanisms accounting for differential α-SMA sub-cellular localization and levels in neuroblastoma-associated CAFs merit further

investigation. Beyond the distribution of α-SMA, the growing awareness of the TME as a key player in cancer progression underscores its role not merely as structural support but as a dynamic regulatory network that actively interacts with tumor cells to support neuroblastoma progression, invasion and treatment resistance. Therefore a comprehensive analysis focusing on the molecular characterization of both stromal cells and structural alterations in the ECM is required to elucidate the mechanisms underlying the invasive and metastatic phenotypes of neuroblastoma.

The dynamic interactions between neuroblastoma and fibroblast cell populations in our MCTS model revealed significant insights into stromal cell organization in response to tumor influence. In MES MCTSs non-activated fibroblasts tended to distribute uniformly with tumor cells, while in the ADR MCTSs, they formed a cohesive cluster to provide structural support in spheroids generation. This dynamic organization reflects the main role of fibroblasts in ensuring tissue integrity and structural maintenance [41]. In contrast, it is known that activated CAFs preferred a more peripheral localization within the MCTS to create a TME that supports tumor growth, invasion and metastasis [42–44]. These findings underscore the critical role of fibroblast activation status in determining the tumor architecture and behavior.

In several solid tumors, CAFs can drive non-invasive cancer cells to distal tissues and organs [24,43]. While in our study it is reasonable to speculate that CAFs primarily enhance and support the intrinsic metastatic potential of MES neuroblastoma cells, observed in vitro and in vivo. Specifically, we found that MES neuroblastoma cells enhanced the proliferation and activation of fibroblasts in CAFs, establishing a tumor-promoting TME. CAF activation, in turn, increased the secretion and reorganization of ECM proteins, including Collagen IV and laminin. Collagen IV is known to stimulate the expression and activation of matrix metalloproteinases able to remodel the ECM components within the basement membrane and tumor stroma, releasing latent growth factors and creating pathways for cancer cell invasion [45–48]. Conversely, ADR neuroblastoma cells, which are less invasive, only minimally activated fibroblasts into CAFs, resulting in limited support for neuroblastoma cell invasion. Moreover, the co-culture with fibroblasts in MCTSs appeared to induce a tumor-suppressive effect, impeding the invasiveness of the ADR SH-SY5Y neuroblastoma cell line. In the presence of ECM, we observed that fibroblasts migrated from the inner core of cell spheroids and reached the outer surface. However, these cells did not invade the surrounding ECM, probably forming a protective barrier that hinders cancer cell dissemination. This protective effect might involve the formation of gap junctions between activated fibroblasts [49].

Our observation was validated using the in vivo zebrafish model, which is a powerful tool for cancer research. The zebrafish model significantly enhances the understanding of metastatic processes by mimicking the complexity of the biological mechanisms in vivo, allowing real-time monitoring of the interactions between cancer cells and TME and providing more robust and comprehensive insights than in vitro models [24]. However, further characterization of patient-derived samples remains essential to clarify the contribution of the stromal compartment and its interaction with neuroblastoma cells, providing a more accurate representation of the role of the TME for cancer cell survival and aggressiveness. Given the ability of fibroblasts to enhance the MES phenotype in neuroblastoma cells observed in our study, future analysis will be essential to determine whether this phenotypic shift is also reflected at the level of MES-specific molecular markers. Additionally, exploring the molecular mechanisms underlying CAF activation promoted by MES neuroblastoma cells could lead to the development of novel strategies aimed at blocking CAF activation and reprogramming them into a non-pathogenic state. These strategies might be critical in reducing the metastatic potential of MES neuroblastoma cells.

Supplementary Materials: The following supporting information can be downloaded at: https://www.mdpi.com/article/10.3390/jnt5040013/s1, Figure S1: Viability of IMR-32 spheroids and the corresponding MCTSs. Representative Z-stack fluorescence images of monoculture spheroids and MCTSs viability (%) at 1 day of culture. MCTSs were stained with Calcein (green, live cells) and EthD-1 (red, dead cells). Scale bars: 100 µm. The mean percentage (%) of viable cells was represented in the histogram on the right. Statistical analysis was conducted between the MCTS and the respective NB monoculture. Data were presented as mean ± SEM, n = 3; Figure S2: The direct cell–cell contact of neuroblastoma cells and fibroblasts induced CAF activation. Representative confocal images of FAP immunostaining (green) in the indicated mono- and co-cultures. Neuroblastoma cells were labeled with the GD2 antibody (red), while nuclei were stained with DAPI (blue). White arrows indicated the cytoplasmic expression of FAP in CAFs. Scale bars: 50 µm; Figure S3: Fibroblasts did not alter the migration properties of neuroblastoma cells. Representative fluorescence images of monoculture and MCTSs of SK-N-AS, IMR-32 and SH-SY5Y with BJ fibroblasts in a wound healing assay upon 6 days of co-culture. Neuroblastoma cells were labeled with Vybrant-DiD (red) while BJ fibroblasts were labeled with Vybrant-DiO (green). The percentage (%) of wound closure at any time point was calculated relative to the initial wound width. Statistical analysis was conducted between the MCTSs and their respective NB monocultures. Data were presented as mean ± SEM, n = 3, ** $p < 0.01$. Scale bar 100 µm.

Author Contributions: Conception and Design: D.C.; Development of Methodology: D.C. and C.N.; Analysis and Interpretation of Data: C.N., D.C., M.P., S.M. and S.A.; Writing: C.N. and D.C.; Revision of the Manuscript: S.A. and A.B. All authors have read and agreed to the published version of the manuscript.

Funding: This work was financially supported by the Fondazione Umberto Veronesi Fellowship—ID 5260 (D.C.) and Associazione Italiana per la Lotta al Neuroblastoma (S.A.).

Data Availability Statement: No new data were created or analyzed in this study. Data sharing is not applicable to this article.

Acknowledgments: The authors thank Fondazione Umberto Veronesi (FUV) and Associazione Italiana per la Lotta al Neuroblastoma for their financial support. We gratefully acknowledge JJ Molenaar (Utrecht University) for providing the 691-ADR and 691-MES neuroblastoma cells. A special acknowledgment goes to Francesca Sensi and Astrid Mollocastillo from University of Padova, who generously provided technical assistance with immunofluorescence stainings.

Conflicts of Interest: The authors declare that they have no conflicts of interest.

References

1. Park, J.R.; Eggert, A.; Caron, H. Neuroblastoma: Biology, Prognosis, and Treatment. *Hematol. Oncol. Clin. N. Am.* **2010**, *24*, 65–86. [CrossRef]
2. Matthay, K.K.; Maris, J.M.; Schleiermacher, G.; Nakagawara, A.; Mackall, C.L.; Diller, L.; Weiss, W.A. Neuroblastoma. *Nat. Rev. Dis. Primer.* **2016**, *2*, 16078. [CrossRef] [PubMed]
3. van Groningen, T.; Koster, J.; Valentijn, L.J.; Zwijnenburg, D.A.; Akogul, N.; Hasselt, N.E.; Broekmans, M.; Haneveld, F.; Nowakowska, N.E.; Bras, J.; et al. Neuroblastoma is composed of two super-enhancer-associated differentiation states. *Nat. Genet.* **2017**, *49*, 1261–1266. [CrossRef] [PubMed]
4. Boeva, V.; Louis-Brennetot, C.; Peltier, A.; Durand, S.; Pierre-Eugène, C.; Raynal, V.; Etchevers, H.C.; Thomas, S.; Lermine, A.; Daudigeos-Dubus, E.; et al. Heterogeneity of neuroblastoma cell identity defined by transcriptional circuitries. *Nat. Genet.* **2017**, *49*, 1408–1413. [CrossRef] [PubMed]
5. Louault, K.; De Clerck, Y.A.; Janoueix-Lerosey, I. The neuroblastoma tumor microenvironment: From an in-depth characterization towards novel therapies. *EJC Paediatr. Oncol.* **2024**, *3*, 100161. [CrossRef]
6. Sengupta, S.; Das, S.; Crespo, A.C.; Cornel, A.M.; Patel, A.G.; Mahadevan, N.R.; Campisi, M.; Ali, A.K.; Sharma, B.; Rowe, J.H.; et al. Mesenchymal and adrenergic cell lineage states in neuroblastoma possess distinct immunogenic phenotypes. *Nat. Cancer* **2022**, *3*, 1228–1246. [CrossRef]
7. Cornel, A.M.; Dunnebach, E.; Hofman, D.A.; Das, S.; Sengupta, S.; Van Den Ham, F.; Wienke, J.; Strijker, J.G.M.; Van Den Beemt, D.A.M.H.; Essing, A.H.W.; et al. Epigenetic modulation of neuroblastoma enhances T cell and NK cell immunogenicity by inducing a tumor-cell lineage switch. *J. Immunother. Cancer.* **2022**, *10*, e005002. [CrossRef] [PubMed]
8. Arina, A.; Idel, C.; Hyjek, E.M.; Alegre, M.-L.; Wang, Y.; Bindokas, V.P.; Weichselbaum, R.R.; Schreiber, H. Tumor-associated fibroblasts predominantly come from local and not circulating precursors. *Proc. Natl. Acad. Sci. USA* **2016**, *113*, 7551–7556. [CrossRef]
9. Werner, S.; Lützkendorf, J.; Müller, T.; Müller, L.P.; Posern, G. MRTF-A controls myofibroblastic differentiation of human multipotent stromal cells and their tumour-supporting function in xenograft models. *Sci. Rep.* **2019**, *9*, 11725. [CrossRef]

10. Orimo, A.; Gupta, P.B.; Sgroi, D.C.; Arenzana-Seisdedos, F.; Delaunay, T.; Naeem, R.; Carey, V.J.; Richardson, A.L.; Weinberg, R.A. Stromal Fibroblasts Present in Invasive Human Breast Carcinomas Promote Tumor Growth and Angiogenesis through Elevated SDF-1/CXCL12 Secretion. *Cell* **2005**, *121*, 335–348. [CrossRef]
11. Räsänen, K.; Vaheri, A. Activation of fibroblasts in cancer stroma. *Exp. Cell Res.* **2010**, *316*, 2713–2722. [CrossRef]
12. Pelon, F.; Bourachot, B.; Kieffer, Y.; Magagna, I.; Mermet-Meillon, F.; Bonnet, I.; Costa, A.; Givel, A.-M.; Attieh, Y.; Barbazan, J.; et al. Cancer-associated fibroblast heterogeneity in axillary lymph nodes drives metastases in breast cancer through complementary mechanisms. *Nat. Commun.* **2020**, *11*, 404. [CrossRef]
13. Costa, A.; Thirant, C.; Kramdi, A.; Pierre-Eugène, C.; Louis-Brennetot, C.; Blanchard, O.; Surdez, D.; Gruel, N.; Lapouble, E.; Pierron, G.; et al. Single-cell transcriptomics reveals shared immunosuppressive landscapes of mouse and human neuroblastoma. *J. Immunother. Cancer* **2022**, *10*, e004807. [CrossRef]
14. Dirat, B.; Bochet, L.; Dabek, M.; Daviaud, D.; Dauvillier, S.; Majed, B.; Wang, Y.Y.; Meulle, A.; Salles, B.; Le Gonidec, S.; et al. Cancer-Associated Adipocytes Exhibit an Activated Phenotype and Contribute to Breast Cancer Invasion. *Cancer Res.* **2011**, *71*, 2455–2465. [CrossRef]
15. Sahai, E.; Astsaturov, I.; Cukierman, E.; DeNardo, D.G.; Egeblad, M.; Evans, R.M.; Fearon, D.; Greten, F.R.; Hingorani, S.R.; Hunter, T.; et al. A framework for advancing our understanding of cancer-associated fibroblasts. *Nat. Rev. Cancer* **2020**, *20*, 174–186. [CrossRef]
16. Zhao, Z.; Li, T.; Sun, L.; Yuan, Y.; Zhu, Y. Potential mechanisms of cancer-associated fibroblasts in therapeutic resistance. *Biomed. Pharmacother.* **2023**, *166*, 115425. [CrossRef] [PubMed]
17. Erdogan, B.; Webb, D.J. Cancer-associated fibroblasts modulate growth factor signaling and extracellular matrix remodeling to regulate tumor metastasis. *Biochem. Soc. Trans.* **2017**, *45*, 229–236. [CrossRef] [PubMed]
18. Wu, F.; Yang, J.; Liu, J.; Wang, Y.; Mu, J.; Zeng, Q.; Deng, S.; Zhou, H. Signaling pathways in cancer-associated fibroblasts and targeted therapy for cancer. *Signal Transduct. Target. Ther.* **2021**, *6*, 218. [CrossRef] [PubMed]
19. Hashimoto, O.; Yoshida, M.; Koma, Y.; Yanai, T.; Hasegawa, D.; Kosaka, Y.; Nishimura, N.; Yokozaki, H. Collaboration of cancer-associated fibroblasts and tumour-associated macrophages for neuroblastoma development. *J. Pathol.* **2016**, *240*, 211–223. [CrossRef] [PubMed]
20. Zeine, R.; Salwen, H.R.; Peddinti, R.; Tian, Y.; Guerrero, L.; Yang, Q.; Chlenski, A.; Cohn, S.L. Presence of cancer-associated fibroblasts inversely correlates with Schwannian stroma in neuroblastoma tumors. *Mod. Pathol.* **2009**, *22*, 950–958. [CrossRef]
21. Borriello, L.; Nakata, R.; Sheard, M.A.; Fernandez, G.E.; Sposto, R.; Malvar, J.; Blavier, L.; Shimada, H.; Asgharzadeh, S.; Seeger, R.C.; et al. Cancer-Associated Fibroblasts Share Characteristics and Protumorigenic Activity with Mesenchymal Stromal Cells. *Cancer Res.* **2017**, *77*, 5142–5157. [CrossRef] [PubMed]
22. Di Matteo, S.; Avanzini, M.A.; Pelizzo, G.; Calcaterra, V.; Croce, S.; Spaggiari, G.M.; Theuer, C.; Zuccotti, G.; Moretta, L.; Pelosi, A.; et al. Neuroblastoma Tumor-Associated Mesenchymal Stromal Cells Regulate the Cytolytic Functions of NK Cells. *Cancers* **2022**, *15*, 19. [CrossRef] [PubMed]
23. van Wezel, E.M.; van Zogchel, L.M.J.; van Wijk, J.; Timmerman, I.; Vo, N.-K.; Zappeij-Kannegieter, L.; de Carolis, B.; Simon, T.; van Noesel, M.M.; Molenaar, J.J.; et al. Mesenchymal Neuroblastoma Cells Are Undetected by Current mRNA Marker Panels: The Development of a Specific Neuroblastoma Mesenchymal Minimal Residual Disease Panel. *JCO Precis. Oncol.* **2019**, *3*, 1–11. [CrossRef]
24. Liu, C.; Zhang, Y.; Lim, S.; Hosaka, K.; Yang, Y.; Pavlova, T.; Alkasalias, T.; Hartman, J.; Jensen, L.; Xing, X.; et al. A Zebrafish Model Discovers a Novel Mechanism of Stromal Fibroblast-Mediated Cancer Metastasis. *Clin. Cancer Res.* **2017**, *23*, 4769–4779. [CrossRef]
25. Horwacik, I. The Extracellular Matrix and Neuroblastoma Cell Communication—A Complex Interplay and Its Therapeutic Implications. *Cells* **2022**, *11*, 3172. [CrossRef] [PubMed]
26. Hanley, C.J.; Noble, F.; Ward, M.; Bullock, M.; Drifka, C.; Mellone, M.; Manousopoulou, A.; Johnston, H.E.; Hayden, A.; Thirdborough, S.; et al. A subset of myofibroblastic cancer-associated fibroblasts regulate collagen fiber elongation, which is prognostic in multiple cancers. *Oncotarget* **2015**, *7*, 6159–6174. [CrossRef]
27. Li, H.; Courtois, E.T.; Sengupta, D.; Tan, Y.; Chen, K.H.; Goh, J.J.L.; Kong, S.L.; Chua, C.; Hon, L.K.; Tan, W.S.; et al. Reference component analysis of single-cell transcriptomes elucidates cellular heterogeneity in human colorectal tumors. *Nat. Genet.* **2017**, *49*, 708–718. [CrossRef]
28. Corrias, M.V.; Parodi, S.; Haupt, R.; Lacitignola, L.; Negri, F.; Sementa, A.R.; Dau, D.; Scuderi, F.; Carlini, B.; Bianchi, M.; et al. Detection of GD2-positive cells in bone marrow samples and survival of patients with localised neuroblastoma. *Br. J. Cancer* **2008**, *98*, 263–269. [CrossRef] [PubMed]
29. Liu, S.; Yin, W.; Lin, Y.; Huang, S.; Xue, S.; Sun, G.; Wang, C. Metastasis pattern and prognosis in children with neuroblastoma. *World J. Surg. Oncol.* **2023**, *21*, 130. [CrossRef]
30. Ara, T.; DeClerck, Y.A. Mechanisms of invasion and metastasis in human neuroblastoma. *Cancer Metastasis Rev.* **2006**, *25*, 645–657. [CrossRef]
31. Desmoulière, A.; Geinoz, A.; Gabbiani, F.; Gabbiani, G. Transforming growth factor-beta 1 induces alpha-smooth muscle actin expression in granulation tissue myofibroblasts and in quiescent and growing cultured fibroblasts. *J. Cell Biol.* **1993**, *122*, 103–111. [CrossRef] [PubMed]
32. Hinz, B.; Celetta, G.; Tomasek, J.J.; Gabbiani, G.; Chaponnier, C. Alpha-Smooth Muscle Actin Expression Upregulates Fibroblast Contractile Activity. *Mol. Biol. Cell* **2001**, *12*, 2730–2741. [CrossRef] [PubMed]

33. Ronnov-Jessen, L.; Petersen, O.W. Induction of alpha-smooth muscle actin by transforming growth factor-beta 1 in quiescent human breast gland fibroblasts. Implications for myofibroblast generation in breast neoplasia. *Lab. Investig. J. Tech. Methods Pathol.* **1993**, *68*, 696–707.
34. Proestler, E.; Donzelli, J.; Nevermann, S.; Breitwieser, K.; Koch, L.F.; Best, T.; Fauth, M.; Wickström, M.; Harter, P.N.; Kogner, P.; et al. The multiple functions of miR-574-5p in the neuroblastoma tumor microenvironment. *Front. Pharmacol.* **2023**, *14*, 1183720. [CrossRef]
35. Goffin, J.M.; Pittet, P.; Csucs, G.; Lussi, J.W.; Meister, J.-J.; Hinz, B. Focal adhesion size controls tension-dependent recruitment of α-smooth muscle actin to stress fibers. *J. Cell Biol.* **2006**, *172*, 259–268. [CrossRef]
36. Hinz, B.; Dugina, V.; Ballestrem, C.; Wehrle-Haller, B.; Chaponnier, C. α-Smooth Muscle Actin Is Crucial for Focal Adhesion Maturation in Myofibroblasts. *Mol. Biol. Cell* **2003**, *14*, 2508–2519. [CrossRef] [PubMed]
37. Liu, C.; Mak, M. Fibroblast-mediated uncaging of cancer cells and dynamic evolution of the physical microenvironment. *Sci. Rep.* **2022**, *12*, 791. [CrossRef]
38. Kumar, S.; Weaver, V.M. Mechanics, malignancy, and metastasis: The force journey of a tumor cell. *Cancer Metastasis Rev.* **2009**, *28*, 113–127. [CrossRef]
39. Patel, A.K.; Vipparthi, K.; Thatikonda, V.; Arun, I.; Bhattacharjee, S.; Sharan, R.; Arun, P.; Singh, S. A subtype of cancer-associated fibroblasts with lower expression of alpha-smooth muscle actin suppresses stemness through BMP4 in oral carcinoma. *Oncogenesis* **2018**, *7*, 1–15. [CrossRef]
40. Talele, N.P.; Fradette, J.; Davies, J.E.; Kapus, A.; Hinz, B. Expression of α-Smooth Muscle Actin Determines the Fate of Mesenchymal Stromal Cells. *Stem Cell Rep.* **2015**, *4*, 1016–1030. [CrossRef]
41. Younesi, F.S.; Miller, A.E.; Barker, T.H.; Rossi, F.M.V.; Hinz, B. Fibroblast and myofibroblast activation in normal tissue repair and fibrosis. *Nat. Rev. Mol. Cell Biol.* **2024**, *25*, 617–638. [CrossRef] [PubMed]
42. Lee, J.-H.; Kim, S.-K.; Khawar, I.A.; Jeong, S.-Y.; Chung, S.; Kuh, H.-J. Microfluidic co-culture of pancreatic tumor spheroids with stellate cells as a novel 3D model for investigation of stroma-mediated cell motility and drug resistance. *J. Exp. Clin. Cancer Res.* **2018**, *37*, 4. [CrossRef]
43. Goulet, C.R.; Champagne, A.; Bernard, G.; Vandal, D.; Chabaud, S.; Pouliot, F.; Bolduc, S. Cancer-associated fibroblasts induce epithelial–mesenchymal transition of bladder cancer cells through paracrine IL-6 signalling. *BMC Cancer* **2019**, *19*, 137. [CrossRef]
44. Wei, X.; Wu, Y.; Chen, K.; Wang, L.; Xu, M. Embedded bioprinted multicellular spheroids modeling pancreatic cancer bioarchitecture towards advanced drug therapy. *J. Mater. Chem. B.* **2024**, *12*, 1788–1797. [CrossRef] [PubMed]
45. Kessenbrock, K.; Plaks, V.; Werb, Z. Matrix Metalloproteinases: Regulators of the Tumor Microenvironment. *Cell* **2010**, *141*, 52–67. [CrossRef]
46. Miyazaki, K.; Oyanagi, J.; Hoshino, D.; Togo, S.; Kumagai, H.; Miyagi, Y. Cancer cell migration on elongate protrusions of fibroblasts in collagen matrix. *Sci. Rep.* **2019**, *9*, 292. [CrossRef] [PubMed]
47. Yamaguchi, H.; Sakai, R. Direct Interaction between Carcinoma Cells and Cancer Associated Fibroblasts for the Regulation of Cancer Invasion. *Cancers* **2015**, *7*, 2054–2062. [CrossRef]
48. Li, X.; González-Maroto, C.; Tavassoli, M. Crosstalk between CAFs and tumour cells in head and neck cancer. *Cell Death Discov.* **2024**, *10*, 1–16. [CrossRef]
49. Omori, Y.; Dagli, M.L.Z.; Yamakage, K.; Yamasaki, H. Involvement of gap junctions in tumor suppression: Analysis of genetically-manipulated mice. *Mutat. Res. Mol. Mech. Mutagen.* **2001**, *477*, 191–196. [CrossRef]

Disclaimer/Publisher's Note: The statements, opinions and data contained in all publications are solely those of the individual author(s) and contributor(s) and not of MDPI and/or the editor(s). MDPI and/or the editor(s) disclaim responsibility for any injury to people or property resulting from any ideas, methods, instructions or products referred to in the content.